Understanding of conversion process of magnetron deposited thin films of amorphous ReO_x to crystalline ReO_3 upon thermal annealing

Boris Polyakov[1], Edgars Butanovs[1], Andrejs Ogurcovs[2], Sergei Vlassov[3], Martins Zubkins[1], Inga Jonane,[1] Arturs Cintins,[1] Aleksandr Kalinko,[1,4] Alexei Kuzmin[1], Juris Purans[1]

[1]Institute of Solid State Physics, University of Latvia, Kengaraga Street 8, LV-1063 Riga, Latvia
[2]G. Liberts' Innovative Microscopy Centre, Department of Technology, Institute of Life Sciences and Technology, Daugavpils University, Parades street 1a, LV-5401 Daugavpils, Latvia
[3] Institute of Physics, University of Tartu, W. Ostwaldi Str. 1, 50412, Tartu, Estonia
[4] Department of Chemistry and Center for Sustainable Systems Design, Paderborn University, 33098 Paderborn, Germany

Keywords
ReO_3, magnetron sputtering, thin film, resistivity, optical, conductive AFM, SEM, XPS, XAS

Abstract

Thin films of rhenium trioxide (ReO_3) were produced by reactive DC magnetron sputtering from metallic rhenium target followed by annealing in the air in the range of temperatures from 200°C to 350°C. Nanocrystalline single-phase ReO_3 films were obtained upon annealing at about 250°C. The thin films appear bright red in reflected light and blue-green in transmitted light, thus showing an optical transparency window in the spectral range of 475-525 nm. The film exhibits high conductivity, evidenced by macro- and nano-scale conductivity measurements. The long-range and local atomic structures of the films were studied in detail by structural methods as X-ray diffraction and X-ray absorption spectroscopy. The oxidation state (6+) of rhenium was confirmed by X-ray photoemission and X-ray absorption spectroscopies. The nanocrystalline morphology of the annealed films was evidenced by scanning electron microscopy (SEM), transmission electron microscopy (TEM) and atomic force microscopy (AFM). The obtained results allowed us to propose the mechanism of rhenium oxide conversion from the initially amorphous ReO_x phase to cubic ReO_3.

1. Introduction

Rhenium oxides are known to exist in the three main phases ReO_2, ReO_3 and Re_2O_7, corresponding to the oxidation states of Re^{4+}, Re^{6+} and Re^{7+}, respectively. ReO_2 is dark blue or black solid and has a monoclinic phase α-ReO_2 below 300°C [1]. When heated above 300°C, it irreversibly turns into the orthorhombic phase β-ReO_2, which is stable in vacuum to 850-1000°C but oxidizes in the air to Re_2O_7 above 400°C. Both phases of ReO_2 have metallic conductivity [2]. Crystalline Re_2O_7 is an inorganic polymer and it is electrically insulating material [2]. It consists of ReO_6 octahedra and ReO_4 tetrahedra. In each octahedral ReO_6 group, three of the Re-O bonds are longer than the others, and if weak bonds are broken (e.g., upon heating) volatile molecules of Re_2O_7 are produced. Re_2O_7 sublimes at temperatures above 360°C. Besides, Re_2O_7 is highly hygroscopic, decomposing into perrhenic acid ($HReO_4$) when exposed to moisture [3]. ReO_3 is a red solid with a metallic luster. Its cubic crystalline structure is of perovskite-type and is formed by a network of regular ReO_6 octahedra, which have common vertices in three

B. Polyakov, E. Butanovs, A. Ogurcovs, S. Vlassov, M. Zubkins, I. Jonane, A. Cintins, A. Kalinko, A. Kuzmin, J. Purans, Understanding the conversion process of magnetron-deposited thin films of amorphous ReOx to crystalline ReO3 upon thermal annealing, Cryst. Growth Des. 20 (2020) 6147-6156. https://doi.org/10.1021/acs.cgd.0c00848

dimensions with the Re–O–Re angles of 180°. Such a structure is often referred to as the ReO_3-type and is found in many materials that were recently reviewed in [4].

Strong Re-O covalent bonds and the $5d^1$ electronic configuration of Re^{6+} ions [5,6] make ReO_3 an intriguing material, sometimes called a "covalent metal", because it has a high metallic conductivity comparable to metals due to the delocalized nature of d-electrons [7–11]. The coupling between phonons and conduction electrons is responsible for the stability of the ReO_3 lattice [12]. As a result, the cubic (*Pm*-3*m*) structure of bulk ReO_3 is undistorted up to its decomposition temperature of about 400°C [13]. At the same time, it undergoes several pressure-induced phase transitions up to 52 GPa [14], which are different in nanocrystalline ReO_3 [15]. Besides, the lattice of bulk ReO_3 demonstrates weak or even negative thermal expansion due to the strong anisotropy of thermal oxygen vibrations [16–18].

Reducing the size of the material can favorably change its properties. Therefore, recent research on ReO_3 at the nanoscale level has been intensified. The synthesis of rhenium oxide nanoparticles was demonstrated using several routes such as decomposition of the Re_2O_7-dioxane complex under solvothermal conditions [19], heating of Re_2O_7 methanolic solution at 250°C sandwiched between two silicon wafer substrates [20,21], radiolytic reduction of sodium perrhenate solutions under gamma irradiation [22], hydrothermal synthesis from ammonium perrhenate solution in methanol [23], and template synthesis using polymer complexes [24]. The growth of ReO_3 nanowires via a simple atmospheric-pressure chemical vapor deposition (APCVD) method at 300 °C has been also reported [25]. The optical properties of metallic ReO_3 nanoparticles with a size below 40 nm are determined to a large extent by a plasmonic band at about 520-530 nm [19,21], which shifts to 860 nm for the larger (60 nm) nanocubes [20]. A few practical applications of ReO_3 nanoparticles are limited to electrocatalysis [23], photocatalysis [20,24], and photothermal antibacterial use [26].

ReO_3 thin films could find more technological applications. However, their production is rather tricky due to the low decomposition temperature of ReO_3 and the possibility of its oxidation to 7+ valence state. To our knowledge, only three articles have been published on this topic so far. The reactive RF sputtering of metallic rhenium target followed by a post-annealing in the Ar atmosphere in the temperature range from 150°C to 300°C was used in [27] to produce a superconductive bilayered film of $NdBa_2Cu_3O_6/ReO_3$. The optimum annealing temperature for the production of conductive (10^{-4} Ω cm) single phase cubic ReO_3 thin films was found to be around 200°C, but the superconductivity was not observed [27]. In other two studies, reactive DC magnetron sputtering was used for the deposition of mixed-valence rhenium oxides [28,29]. The absorption features and the colour change of the films from golden brown to red suggest that the films mainly contain the ReO_3 phase with some oxygen non-stoichiometry [28]. Mixed-valent rhenium oxide thin films were deposited using reactive DC magnetron sputtering from a metallic rhenium target in an oxygen-argon atmosphere [29]. X-ray photoelectron spectroscopy confirmed that all films consisted largely of ReO_3, but had some contributions from Re_2O_3, ReO_2 and Re_2O_7 [29].

In this study, we performed a comprehensive investigation of ReO_3 thin films produced by reactive DC magnetron sputtering and subsequent annealing in air at different temperatures. The structure and morphology of the films, as well as their optical and electrical properties, were characterized and discussed.

B. Polyakov, E. Butanovs, A. Ogurcovs, S. Vlassov, M. Zubkins, I. Jonane, A. Cintins, A. Kalinko, A. Kuzmin, J. Purans, Understanding the conversion process of magnetron-deposited thin films of amorphous ReOx to crystalline ReO3 upon thermal annealing, Cryst. Growth Des. 20 (2020) 6147-6156. https://doi.org/10.1021/acs.cgd.0c00848

2. Experimental procedure

Rhenium oxide ReO_3 thin films were prepared by reactive DC magnetron sputtering and followed by annealing in air. The target was metal Re disc of 99.9% purity 50 cm in diameter and 0.3 mm thick (*GoodFellow*). The substrates were 25x25 mm fused quartz glasses (*SPI supplies*) and 25x25 mm silicon wafer samples with 50 nm SiO_2 (*Semiconductor Wafers Inc.*). Magnetron sputtering was performed in the vacuum system *SAF25/50* (*Sidrabe*) for 10 minutes at 100 W DC magnetron power in a mixed atmosphere of sputtering Ar gas (20 sccm) and reactive O_2 gas (10 sccm) at total pressure 20 mTorr. The substrate was at room temperature during the deposition process. Half an hour annealing at 200°C, 250°C and 300°C in air atmosphere was performed to obtain ReO_3. During annealing clean piece of quartz or silicon was placed on the sample surface to avoid evaporation of rhenium oxide (see Fig.S1 in Supplementary Data). If samples are heated without capping the rhenium oxide films start to sublime and disappear. A commercial ReO_3 powder (from Metalli Preziosi S.p.A., 99.9% pure) and ReO_2 (Sigma-Aldrich, 99.7% pure) were used as references.

The crystal structure of rhenium oxide films was studied by X-ray diffraction (XRD) at room temperature using a powder diffractometer *MiniFlex 600* equipped with copper anode X-ray tube (*Rigaku*). The film morphology was studied by a scanning electron microscope SEM/FIB *Lyra XM* (*Tescan*) in SE (secondary electrons) regime. The crystalline structure of the of rhenium oxide film annealed at 250°C was using a transmission electron microscope (TEM, Tecnai GF20, FEI) operated at a 200 kV accelerating voltage. SAED analysis was perfomed using CrysTBox diffractGUI 2.21 software (written by Miloslav Klinger). Thickness values were obtained using a stylus profilometer *Dektak 150* (*Veeco*). Measured thickness for as prepared thin film was 100 nm. The electrical parameters were measured in the Van der Pauw configuration using a Hall effect system, HMS5000 (*Ecopia*). Topography and related electric current maps were obtained in contact mode by atomic force microscope AFM *Park NX10* (*Park Systems*). Optical reflection and transmission spectra were measured using spectrophotometer *Cary 7000* (*Agilent*). The samples were placed at an angle of 6 degrees against the incident beam, and the detector was placed at 180 degrees behind the sample to measure transmittance and at 12 degrees in front of the sample to measure specular reflectance. XPS measurements were performed using an X-ray photoelectron spectrometer *ESCALAB Xi* (ThermoFisher), and XPSPEAK41 software was used for peak fitting.

X-ray absorption spectroscopy (XAS) measurements were performed at room temperature at the Re L_3-edge in the fluorescence (for the films) and transmission (for the reference powders) modes at the HASYLAB/DESY PETRA-III P64 beamline [30]. The X-ray beam from the undulator was monochromatized by Si(311) double-crystal monochromator, and its intensity was recorded using the gas-filled ionization chambers located before and after the sample and the Passivated Implanted Planar Silicon (PIPS) detector (Canberra) placed at 90° to the beam direction close to the sample position. The thin film samples were mounted at 45° to the beam. The reference powders were deposited on Millipore filters, and their weight was chosen to give the value of the absorption edge jump close to 1.0.

3. Reverse Monte Carlo calculations

B. Polyakov, E. Butanovs, A. Ogurcovs, S. Vlassov, M. Zubkins, I. Jonane, A. Cintins, A. Kalinko, A. Kuzmin, J. Purans, Understanding the conversion process of magnetron-deposited thin films of amorphous ReOx to crystalline ReO3 upon thermal annealing, Cryst. Growth Des. 20 (2020) 6147-6156. https://doi.org/10.1021/acs.cgd.0c00848

X-ray absorption spectra of rhenium oxide thin films and reference c-ReO_3 powder recorded at the Re L_3-edge were analyzed using the reverse Monte Carlo (RMC) method based on the evolutionary algorithm (EA), implemented in the EvAX code [31]. The use of the RMC approach is required due to a strong overlap of the outer coordination shells and the presence of multiple-scattering contributions [32].

The extended X-ray absorption fine structures (EXAFS) $\chi(k)k^2$ were extracted using a conventional procedure [33]. Further, the RMC simulation boxes (supercells) having a different size (4a×4b×4c for the as-deposited film and 5a×5a×5a for c-ReO_3 and the annealed film) with periodic boundary conditions (PBC) were constructed based on the rhenium oxide crystallographic structures [34]. RMC/EA calculations were simultaneously performed for 32 atomic configurations. At each iteration, the new atomic configuration was generated by randomly displacing all atoms in the simulation box with a maximum permissible shift of 0.4 Å to obtain the best possible agreement between the Morlet wavelet transforms (WTs) of the experimental and calculated Re L_3-edge EXAFS spectra [35]. The calculations were performed in the *k*-space range of 3.0-12.0 $Å^{-1}$ and the *R*-space range of 0.2-4.0 Å for the as-deposited film, whereas in the *k*-space range of 2.0-12.0 $Å^{-1}$ and the *R*-space range of 1.0-6.0 Å for c-ReO_3 and the annealed film. After 5000 iterations, no significant improvement in the residual was observed. To improve statistics, the RMC simulations were repeated several times using different sequences of random numbers.

The configuration-averaged EXAFS spectra were calculated by ab initio real-space multiple-scattering (MS) FEFF8.50L code [36,37], including the MS effects up to 7th order. The scattering potential and partial phase shifts were calculated only once in the muffin-tin (MT) approximation [36,37] for a cluster with a radius of 5.0 Å, centered on the absorbing rhenium atom and constructed based on rhenium oxide crystallographic structures [34]. Small variations of the cluster potential due to atom displacements during the RMC/EA simulations were neglected. The photoelectron inelastic losses were taken into account in the one-plasmon approximation using the complex exchange-correlation Hedin-Lundqvist potential [38]. The amplitude reduction factor S_0^2 is included in the scattering amplitude [36,37], calculated by the FEFF code, and no additional correction of the EXAFS amplitude was performed.

4. Results and Discussion

The as-deposited rhenium oxide films have a shiny gray-gold colour. After annealing at 200°C for 0.5 h the film colour was almost the same. Films annealed at 250°C and 300°C became bright red and blue-green in reflected and transmitted light respectively (Fig. S2 in Supplementary Data). The results of optical reflection and transmission measurements for several annealing temperatures are shown in Fig. 1. Optical measurements confirm the presence of a transparency window in the spectral range of 475-525 nm. The highest transparency of approximately 45% at 530 nm and the minimum reflectivity in the range of 390-460 nm were achieved for the sample annealed at 250°C (Fig.1), which agrees well with results obtained by [28]. The high absorption below 530 nm is associated with interband transitions and above 530 nm due to the free-electrons [29].

B. Polyakov, E. Butanovs, A. Ogurcovs, S. Vlassov, M. Zubkins, I. Jonane, A. Cintins, A. Kalinko, A. Kuzmin, J. Purans,
Understanding the conversion process of magnetron-deposited thin films of amorphous ReOx to crystalline ReO3 upon thermal annealing,
Cryst. Growth Des. 20 (2020) 6147-6156. https://doi.org/10.1021/acs.cgd.0c00848

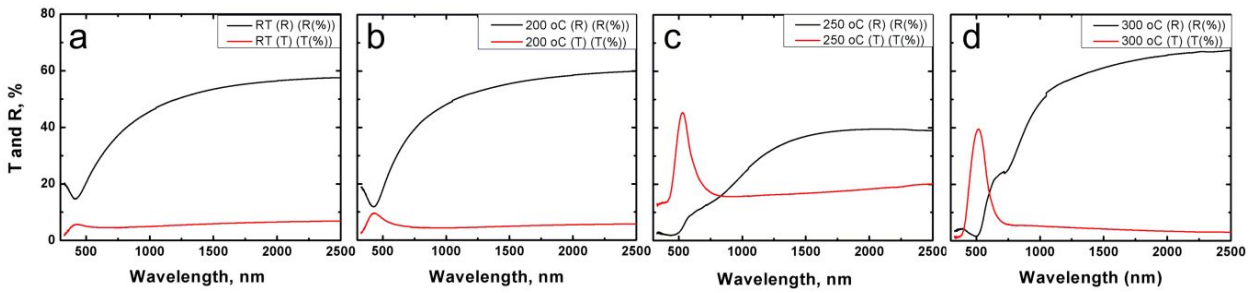

Fig.1. Optical reflection and transmission spectra for as prepared (a) and annealed at 200°C (b), 250°C (c) and 300°C (d) rhenium oxide thin films on quartz slides.

To confirm the presence of the rhenium trioxide ReO_3 phase in the prepared samples, the XRD measurements were performed on the films deposited on oxidized silicon substrates and annealed at different temperatures. The results of XRD measurements are shown in Fig. 2. The as-prepared thin film is X-ray amorphous as its pattern does not contain any Bragg peaks. The only visible Bragg peak at 33° is attributed to the forbidden Si(200) reflection of the Si(100) substrate. From 200°C, diffraction peaks related to the ReO_3 phase start to appear and have the strongest intensity for the sample annealed at 250°C. The presence of the cubic ReO_3 phase was confirmed by diffraction peaks at 24° (100), 32.5° (110), 42° (111), 48° (200) and 54° (210), in agreement with the Powder Diffraction File JCPDS-ICDD 04-014-6505 [14]. According to Rietveld analysis of XRD data the lattice parameter for ReO3 thin films is equal to 3.75 Å. It is interesting to note that the presence of solid perrhenic acid monohydrate [3] is evidenced from the Bragg peaks at 16.6° and 25.5° which are observed on XRD patterns of all annealed films, but not freshly prepared film (RT).

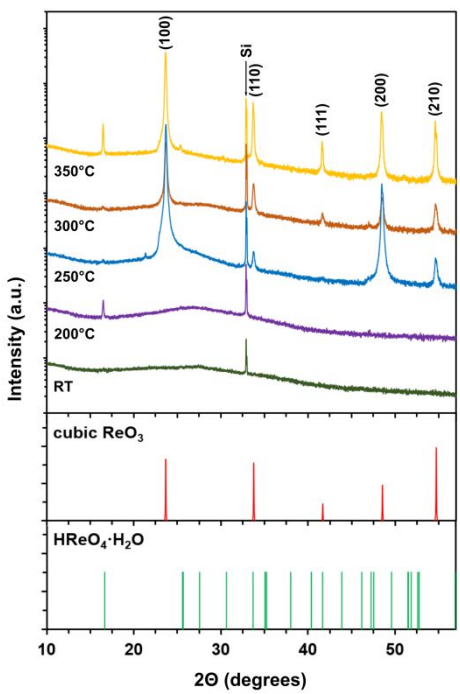

B. Polyakov, E. Butanovs, A. Ogurcovs, S. Vlassov, M. Zubkins, I. Jonane, A. Cintins, A. Kalinko, A. Kuzmin, J. Purans, Understanding the conversion process of magnetron-deposited thin films of amorphous ReOx to crystalline ReO3 upon thermal annealing, Cryst. Growth Des. 20 (2020) 6147-6156. https://doi.org/10.1021/acs.cgd.0c00848

Fig. 2. X-ray diffraction patterns of rhenium oxide thin films on oxidized silicon substrates at the different annealing temperatures. The position of the Bragg peaks for cubic ReO_3 [14] and $HReO_4$ [3] phases are shown by vertical bars.

An XPS study was performed to qualitatively determine the composition of the thin film surface and analyze the valence states of Re atoms. The survey scan (see Fig.S3 in Supplementary Data) indicates the presence only of Re and O elements, as well as a small amount of adventitious carbon. High-resolution spectra of Re 4f peaks (Fig. 3) were acquired to determine the chemical states of rhenium oxide at different thin film preparation temperatures. XPS spectra of O1s for rhenium oxide films are less informative and placed in Supplementary Data (Fig.S4). The spectra were calibrated relative to adventitious C 1s peak at 284.8 eV. To mitigate the error during the peak fitting, spin-orbit splitting of 2.42 eV was fixed between the Re $4f_{7/2}$ and $4f_{5/2}$ components, and the area ratio was held at 4:3. Spectra of sputter-deposited thin films and films annealed at 200°C exhibit three different Re oxidation states. Re $4f_{7/2}$ peak energies at binding energies of 42.90 eV, 43.53 eV and 46.01 eV correspond to 4+, 6+ and 7+ oxidation states, respectively, therefore, indicating the presence of ReO_2, ReO_3 and Re_2O_7 compounds at the surface of the film. The obtained peak values are in good agreement with the ones reported in the literature [39,40]. Typically, the surface of ReO_2 is covered with approximately 2 nm thick surface layer of ReO_3 and Re_2O_3 mixture when exposed to air [39], which presumably can be observed in our measurements. XPS spectra of the samples annealed at 250°C, 300°C and 350°C consists of Re^{6+} and Re^{7+} peaks only and do not contain Re^{4+} peaks at the lower binding energies indicating that at the given temperatures ReO_2 conversion to the higher valence state ReO_3 compound occurs. The Re_2O_7 surface layer is still present in the films; the signal of Re^{7+} from Re_2O_7 can always be detected from ReO3 powders [39]. These surface contaminants exhibit broader and less resolved features due to the high degree of disorder and defects. However, the distinct peaks of ReO_2 in thin-film samples annealed at temperatures up to 200°C and peaks of ReO_3 in samples annealed at 250°C and higher are well resolved and reliable.

B. Polyakov, E. Butanovs, A. Ogurcovs, S. Vlassov, M. Zubkins, I. Jonane, A. Cintins, A. Kalinko, A. Kuzmin, J. Purans,
Understanding the conversion process of magnetron-deposited thin films of amorphous ReOx to crystalline ReO3 upon thermal annealing,
Cryst. Growth Des. 20 (2020) 6147-6156. https://doi.org/10.1021/acs.cgd.0c00848

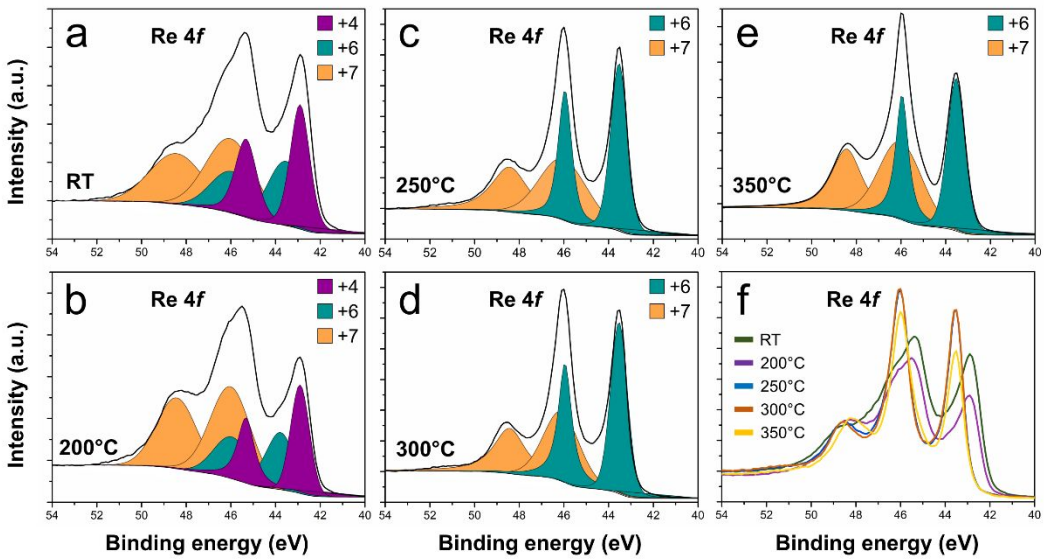

Fig. 3. High-resolution XPS spectra of Re 4*f* peaks of rhenium oxide thin films at different annealing temperatures. Measured Re $4f_{7/2}$ peak energies at 42.90 eV, 43.53 eV and 46.01 eV correspond to 4+, 6+ and 7+ oxidation states, respectively.

The electrical resistivity of the rhenium oxide films was measured in the temperature range 80-350 K in the Van der Pauw configuration using a Hall measurement system (Fig. 4). Current-voltage characteristics were linear for all samples, indicating good ohmic contacts. According to Fig. 4a the resistivity measured at 300K initially decreases with the increase of annealing temperature reaching a minimum value of 4.0×10^{-5} Ωcm at 250°C, and then starts to grow when the annealing temperature is further increased. Minimum resistivity value is better than typical values for ITO films [41] being comparable with some metal thin films [42] and is in a good agreement with [43]. It is interesting to compare the resistivity dependence on temperature for 200°C and 250°C samples. The sample annealed at 200°C shows a resistance decrease with the increase of the temperature (Fig. 4b). Identical behavior is observed also for the RT sample. The sample annealed at 250°C, in contrast, shows a resistance increase with temperature (behavior typical for metals). The measurements do not give stable Hall voltage values as carrier concentrations values (> 10^{21} cm^{-3}) exceed the measurable range of the system.

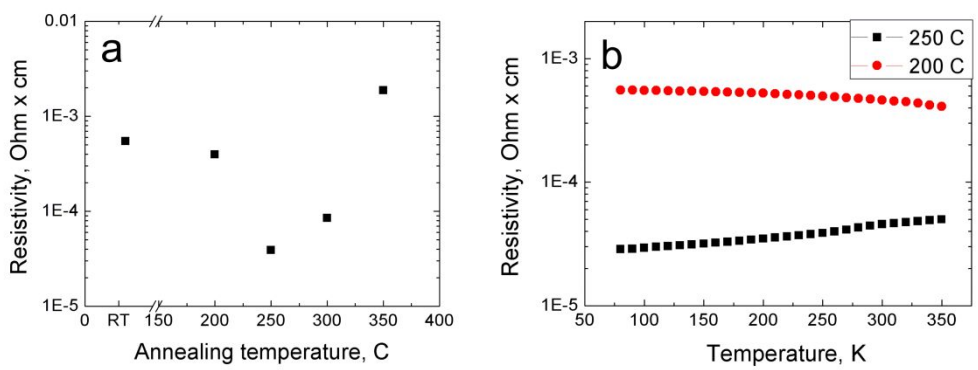

B. Polyakov, E. Butanovs, A. Ogurcovs, S. Vlassov, M. Zubkins, I. Jonane, A. Cintins, A. Kalinko, A. Kuzmin, J. Purans, Understanding the conversion process of magnetron-deposited thin films of amorphous ReOx to crystalline ReO3 upon thermal annealing, Cryst. Growth Des. 20 (2020) 6147-6156. https://doi.org/10.1021/acs.cgd.0c00848

Fig. 4. The resistivity of the rhenium oxide films annealed at different temperatures measured at 300 K (a); temperature dependence of resistivity for the films annealed at 200°C and 250°C (b).

The same set of rhenium oxide films annealed at different temperatures was imaged using SEM microscopy (Fig. 5). Contrary to the X-ray amorphous pattern in XRD measurements of the RT sample, small crystallites can be seen in SEM image (Fig. 5a). These crystals are expected to be Re_2O_7 (see discussion on C-AFM measurements below). The sample annealed at 200°C seems to be similar to the RT sample, however, the average size of crystallites on the sample surface is smaller (Fig. 5b). Drastic morphology change can be seen in the sample annealed at 250°C (Fig. 5c). The film consists of parallelepiped shaped nanocrystals of different sizes and orientations. Further increase of annealing temperature to 300°C leads to another significant decrease in the average crystallite size (Fig. 5d). Morphological changes observed from 250°C to 300°C can explain the increase of film resistivity (Fig. 4): electron scattering is increased with the decrease of ReO_3 nano- or microcrystal size.

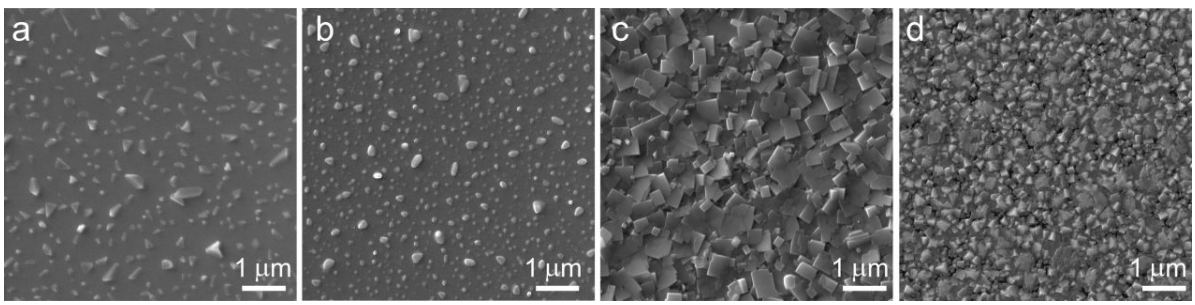

Fig. 5. SEM images of rhenium oxide films: as is (a), annealed at 200° (b), 250° (c), 300°C (d).

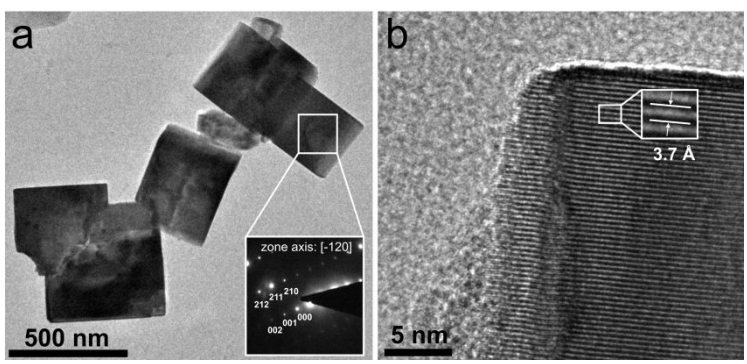

Fig. 6. TEM images of fragment pf rhenium oxide film annealed at 250° C at small (a) and high maginification (b).

TEM microscopy study was performed on small fragments of ReO_3 film prepared at 250° C (fig.6). TEM reveals square shaped ReO_3 nanocrystals of size 100-500 nm. According to high resolution TEM image interplanar distance is 3.7 Å (fig.6b), which is in good agreement with SAED data analysis (fig.6a). SAED analysis confirmed the cubic structure of ReO_3 film.

Conductivity maps and corresponding topography images obtained with conductive AFM in contact mode are shown in Fig. 7. A lot of small nonconducting nanocrystals can be seen at the surface of the as-prepared sample (Fig. 7a,b). These nanocrystals were relatively easy to displace with AFM tip during the scan indicating that they are

B. Polyakov, E. Butanovs, A. Ogurcovs, S. Vlassov, M. Zubkins, I. Jonane, A. Cintins, A. Kalinko, A. Kuzmin, J. Purans, Understanding the conversion process of magnetron-deposited thin films of amorphous ReOx to crystalline ReO3 upon thermal annealing, Cryst. Growth Des. 20 (2020) 6147-6156. https://doi.org/10.1021/acs.cgd.0c00848

not embedded into the film but are situated on the surface. These crystals are probably Re_2O_7, which had grown on the rhenium oxide surface after its exposure to ambient moisture (Re_2O_7 is nonconductive and it is known that Re_2O_7 nanocrystals grow on metallic rhenium surface upon exposure to the atmosphere [1]). After heating to 200°C the number of nonconductive nanocrystals on the surface was greatly reduced (few nonconductive spots are still seen in Fig. 5d). At the same time, bigger and conductive crystals appeared (dark features in Fig. 7d) that can be already seeds of ReO_3. Sample annealed at 250°C demonstrated the highest conductivity despite film defects – nonconductive regions of the pure silicon substrate (Fig. 7f). Sample annealed at 300°C was also highly conductive and had better surface coverage without film defects (Fig. 7h).

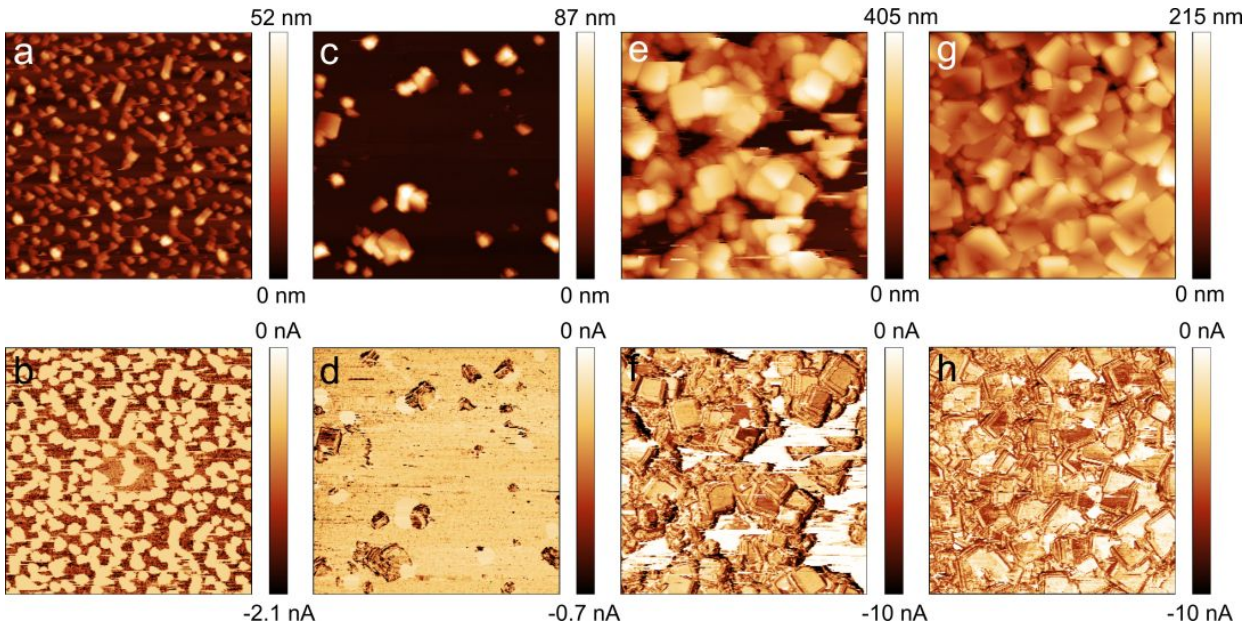

Fig. 7. Topography and conductivity maps 5x5 μm^2 measured with conductive AFM. Sample as prepared (a, b), annealed at 200° (c, d), 250° (e,f), and 300°C (g, h). Applied bias voltage -10 mV. Additionally, 1x1 μm^2 C-AFM images are presented in Fig.S5 in the Supplementary Data file.

Using obtained microscopy and spectroscopy data we sketched a schematics of ReO_3 film growth depending on annealing temperature (Fig. 8). The initial film produced by reactive DC magnetron sputtering is X-ray amorphous. Upon exposure to atmospheric air small crystals of Re_2O_7 start to grow on the film surface (Fig. 8a). After annealing the film at 200°C small crystals of ReO_3 start to grow, while crystals of Re_2O_7 start to disappear (Fig. 8b). The films annealed at 250°C and 300°C consist completely of ReO_3 nanocrystals, however, nanocrystal size at 300°C is smaller and more randomly oriented (Fig. 8c,d).

B. Polyakov, E. Butanovs, A. Ogurcovs, S. Vlassov, M. Zubkins, I. Jonane, A. Cintins, A. Kalinko, A. Kuzmin, J. Purans, Understanding the conversion process of magnetron-deposited thin films of amorphous ReOx to crystalline ReO3 upon thermal annealing, Cryst. Growth Des. 20 (2020) 6147-6156. https://doi.org/10.1021/acs.cgd.0c00848

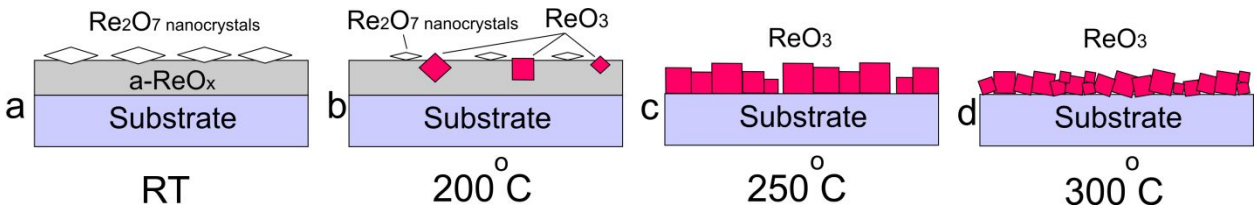

Fig. 8. Schematics of ReO_3 film growth. Small crystals of Re_2O_7 appears on the surface of as-deposited amorphous ReO_x film (a). Upon annealing at 200°C Re_2O_7 start to disappear, while small crystals of ReO_3 start to grow (b). The film of the sample annealed at 250°C is completely formed from ReO_3 nanocrystals (c). The film of the sample annealed at 300°C is also formed from ReO_3 nanocrystals but with smaller size and more randomly oriented (c).

X-ray absorption near edge structure (XANES) spectra of the as-prepared and annealed in air at 250°C thin films and crystalline cubic c-ReO_3 are shown in Fig. 9(a). All three XANES spectra are dominated by a prominent white line peak due to the dipole allowed transition $2p_{3/2}(Re) \rightarrow 5d(Re)+2p(O)$ [13]. The oscillations beyond the white line belong to the extended X-ray absorption fine structure (EXAFS), containing information on the local atomic structure and lattice dynamics [32,44]. The XANES spectra of the annealed film and c-ReO_3 are nearly identical, whereas the spectrum of the as-prepared film differs, in particular, the absorption edge is shifted to lower energies indicating the lower oxidation state of rhenium ions, in agreement with our XPS results (Fig. 3).

Experimental Re L_3-edge EXAFS spectra $\chi(k)k^2$ and their Fourier transforms (FTs) for the four samples are compared in Fig. 9(b,c). Note that all FTs were not corrected for any phase shifts; therefore, the positions of peaks differ from crystallographic values.

The EXAFS spectrum of the as-prepared film is strongly damped at large k-values suggesting the rather strongly disordered structure of the film. This conclusion agrees well with the absence of the Bragg peaks in the diffraction pattern of the film (Fig. 2). Besides, the EXAFS spectrum of the as-prepared film shows some similarity to that of orthorhombic o-ReO_2: all peaks in FTs of both samples are located at close positions but the amplitude of the FT peaks for the film is strongly reduced, reflecting disorder present in the film. Again the local structure of rhenium ions in the film suggests that its oxidation state is 4+ agreeing with the position of the absorption edge. The similarity of the local environment in as-prepared film and orthorhombic o-ReO_2 was used by us to construct the initial structural model for RMC modelling of the film based on the crystallographic structure of o-ReO_2 [2].

After annealing at 250°C, the EXAFS spectra of the film becomes very close to that of cubic c-ReO_3 indicating the similarity of the local environment around Re ions in two samples. The first peak at 1.4 Å in Fig. 9(c) corresponds to the first coordination shell of Re, which is composed of six oxygen atoms. The second peak at 2.8 Å has a complex origin and contains contributions from the multiple-scattering (MS) effects generated in the first shell with some admixture of the second shell [32]. The third peak at 3.6 Å includes mainly contributions from the second shell composed of 6 rhenium atoms (including strong MS signals generated within nearly linear Re-O-Re atomic chains) with some admixture from the third shell composed of 24 oxygen atoms [32]. The last peak at 5 Å contains mainly

B. Polyakov, E. Butanovs, A. Ogurcovs, S. Vlassov, M. Zubkins, I. Jonane, A. Cintins, A. Kalinko, A. Kuzmin, J. Purans, Understanding the conversion process of magnetron-deposited thin films of amorphous ReOx to crystalline ReO3 upon thermal annealing, Cryst. Growth Des. 20 (2020) 6147-6156. https://doi.org/10.1021/acs.cgd.0c00848

contributions from 6 rhenium atoms of the fourth shell and 32 oxygen atoms located in the fifth and sixth shells. The strong MS contributions, which are present due to the cubic structure of perovskite c-ReO_3, complicate the analysis of the Re L_3-edge EXAFS spectra [32,44]. To address this problem, we have successfully employed the reverse Monte Carlo method with an evolutionary algorithm (EA) approach [31].

The results of the RMC fits for three samples are shown in Fig. 10. Good agreement between experimental and best-fitted EXAFS spectra was found both in the k- and R-space supporting the reliability of the obtained structural models. The coordinates of atoms in the RMC simulation box were used to calculate the partial radial distribution functions (RDFs) g(R) and the mean-square relative displacement (MSRD) factors σ^2 for Re-O and Re-Re atom pairs (Fig. 11). Note that the RMC method allowed us to access structural data from the outer coordination shells located up to 6 Å.

The structure of the as-deposited film was simulated starting from the o-ReO_2 one, in which Re^{4+} ions are octahedrally coordinated by oxygen atoms (4 atoms at 1.94 Å and 2 atoms at 2.11 Å), and the nearest ReO_6 octahedra are joined by edges with the mean distance Re-Re=2.61 Å [2]. This structural model fits nicely the EXAFS spectrum of the film, and the strong broadening of the peaks in the partial RDFs g(R) for Re-O and Re-Re atom pairs is consistent with the amorphous structure of the film as seen by XRD (Fig. 2). However, the first peak in the RDF for the Re-O atom pairs contains a well visible peak at 1.76 Å. Such short bonds are absent in the o-ReO_2 structure and reflect strong distortions of the ReO_6 octahedra in the film, presumably, being the source of its amorphous structure. Note also that such short Re-O distances are typical for tetrahedral rhenium coordination [3,45]. Therefore, one can also assume the presence in the film of undercoordinated ReO_x units being responsible for the structural disorder, similar to the case of amorphous TiO_2 [46,47].

A comparison of the RDFs for the thin film annealed at 250°C and crystalline c-ReO_3 indicates that the main difference between them appears in the first coordination shell (Fig. 11(b)). Stronger disorder in the film leads to the first shell larger broadening, which results in a decrease of the first peak amplitude in FT (Fig. 9(c)). The values of the MSRD factors σ^2 in the first five coordination shells of rhenium atoms in both samples are shown in Fig. 11(c). One can note that the MSRD in the film is always slightly larger than in crystalline c-ReO_3 due to the presence of structural disorder in the film. In both cases, the MSRD increases for longer distances due to the loss of correlation in atomic vibrations [48].

B. Polyakov, E. Butanovs, A. Ogurcovs, S. Vlassov, M. Zubkins, I. Jonane, A. Cintins, A. Kalinko, A. Kuzmin, J. Purans,
Understanding the conversion process of magnetron-deposited thin films of amorphous ReOx to crystalline ReO3 upon thermal annealing,
Cryst. Growth Des. 20 (2020) 6147-6156. https://doi.org/10.1021/acs.cgd.0c00848

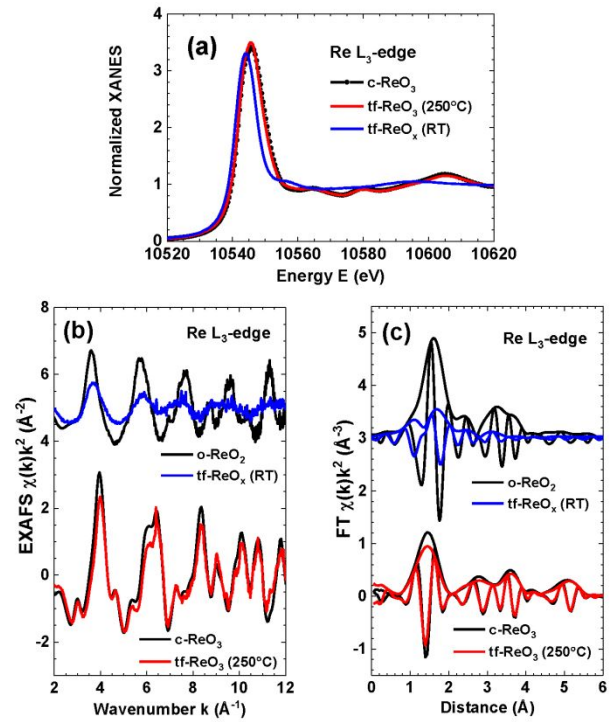

Fig. 9. Experimental Re L_3-edge XANES (a), EXAFS $\chi(k)k^2$ (b) and their Fourier transforms (c) for the as-prepared (RT) and annealed in air at 250°C thin films (tf), cubic c-ReO_3 and orthorhombic o-ReO_2. The curves in (b) and (c) are vertically shifted for clarity.

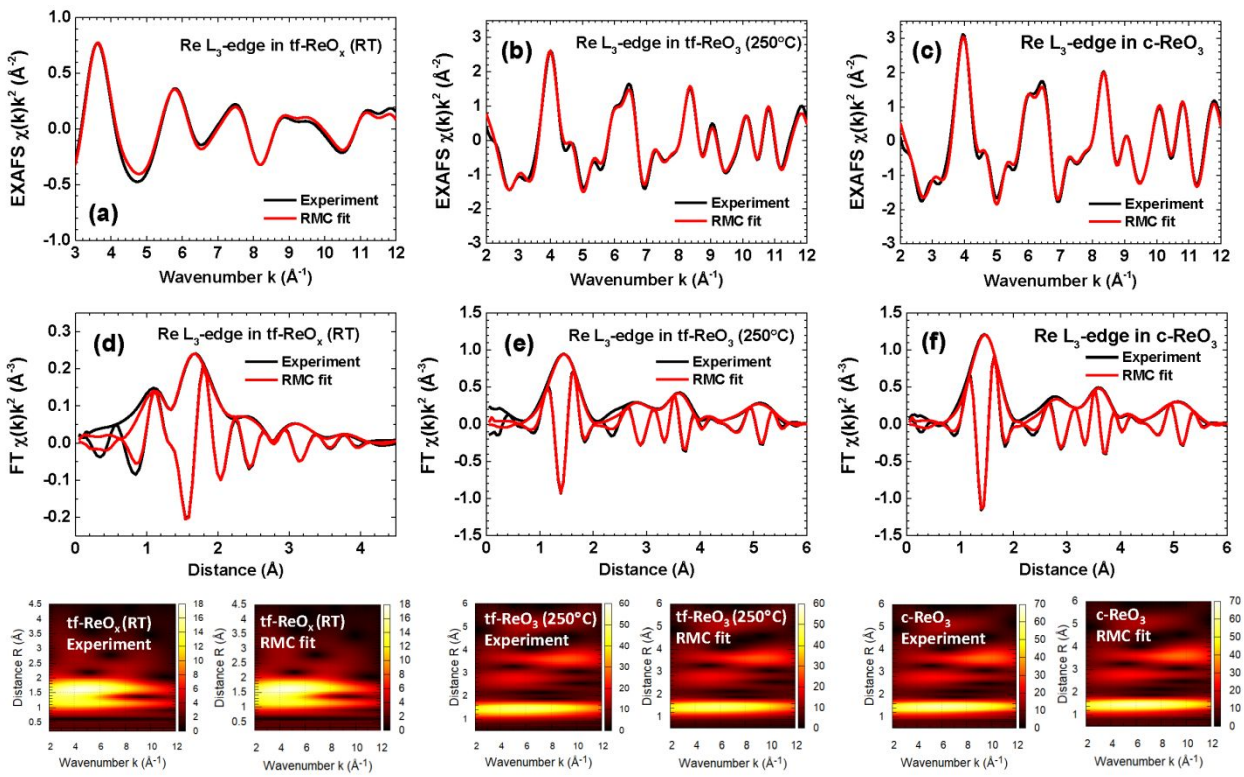

B. Polyakov, E. Butanovs, A. Ogurcovs, S. Vlassov, M. Zubkins, I. Jonane, A. Cintins, A. Kalinko, A. Kuzmin, J. Purans, Understanding the conversion process of magnetron-deposited thin films of amorphous ReOx to crystalline ReO3 upon thermal annealing, Cryst. Growth Des. 20 (2020) 6147-6156. https://doi.org/10.1021/acs.cgd.0c00848

Fig. 10. Comparison of the experimental and RMC fitted Re L_3-edge EXAFS spectra $\chi(k)k^2$ (a-c) and their Fourier and Morlet wavelet transforms (d-f) for the as-prepared (RT) and annealed in air at 250°C thin films (tf) and c-ReO_3.

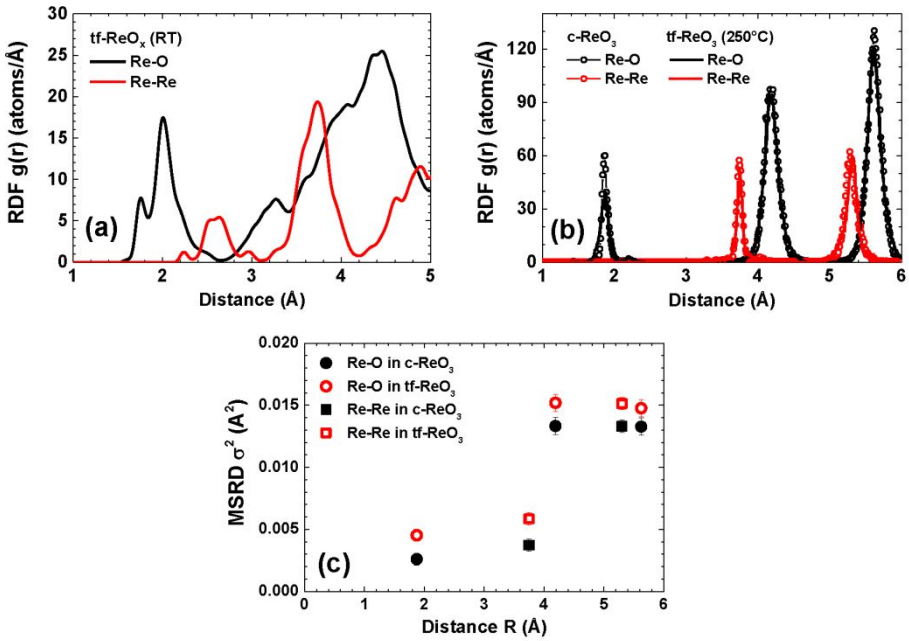

Fig. 11. (a,b) Partial radial distribution functions (RDFs) and (c) the mean-square relative displacements (MSRDs) σ^2 for Re-O and Re-Re atom pairs for the as-prepared (RT) and annealed in air at 250°C thin films (tf) and c-ReO_3.

5. Conclusions

A comprehensive investigation of rhenium oxide thin film growth has been performed to elucidate the mechanisms of the ReO_3 formation upon thermal annealing from amorphous ReO_x produced by reactive DC magnetron sputtering. We found that the as-prepared films are X-ray amorphous, but they readily crystallize upon annealing in the range of temperatures from 200°C to 350°C. Nanocrystalline single-phase ReO_3 films were produced when heated to about 250°C. The nanocrystalline morphology of the annealed films was evidenced by XRD spectroscopy, scanning and transmission electron microscopy, and atomic force microscopy. The metallic nature of the films was confirmed by macro- and nano-scale conductivity measurements. The ReO_3 films demonstrated optical properties typical for thin metallic layers. They appear bright red in reflected light and blue-green in transmitted light, being transparent in the spectral range of 475-525 nm. The local atomic structure of the films was studied by X-ray absorption spectroscopy (XANES/EXAFS). The analysis of the Re L_3-edge EXAFS spectra using the reverse Monte Carlo method suggests that the local atomic structure around rhenium atoms in the as-prepared films is strongly disordered and resembles that in o-ReO_2, whereas the local structure of the thin film annealed in the air at 250°C is close to the one in crystalline c-ReO_3 but is slightly more disordered, reflecting the nanocrystalline morphology of the films. The oxidation state of rhenium ions close to 4+ in the as-prepared film and 6+ in the annealed one was confirmed by XANES and X-ray photoemission spectroscopies. The obtained results allowed us to understand the

B. Polyakov, E. Butanovs, A. Ogurcovs, S. Vlassov, M. Zubkins, I. Jonane, A. Cintins, A. Kalinko, A. Kuzmin, J. Purans, Understanding the conversion process of magnetron-deposited thin films of amorphous ReOx to crystalline ReO3 upon thermal annealing, Cryst. Growth Des. 20 (2020) 6147-6156. https://doi.org/10.1021/acs.cgd.0c00848

mechanism of rhenium oxide conversion from the initially amorphous ReO_x phase to cubic crystalline ReO_3 under annealing.

Acknowledgments

Financial support was provided by ERAF Project Nr. 1.1.1.1/18/A/073. Parts of this research were carried out at PETRA-III P64 beamline at DESY, a member of the Helmholtz Association (HGF). The synchrotron experiments have been supported by the project CALIPSOplus under the Grant Agreement 730872 from the EU Framework Programme for Research and Innovation HORIZON 2020.

Supporting information

This document contains schematics of ReO_3 thin film preparation, optical photos of the as-prepared and annealed rhenium oxide thin films on silicon wafer, XPS survey scan and XPS spectra of O1s for rhenium oxide films annealed at different temperatures, and additional C-AFM data for 1x1 μm^2 scan size for rhenium oxide films.

References

[1] J.M. Mannion, M.S. Wellons, C.R. Shick, G.A. Fugate, B.A. Powell, S.M. Husson, Ambient aging of rhenium filaments used in thermal ionization mass spectrometry: Growth of oxo-rhenium crystallites and anti-aging strategies, Heliyon 3 (2017) e00232. https://doi.org/10.1016/j.heliyon.2017.e00232.

[2] D. Adler, Insulating and Metallic States in Transition Metal Oxides, in: Solid State Phys., Elsevier, 1968: pp. 1–113. https://doi.org/10.1016/S0081-1947(08)60739-0.

[3] G. Wltschek, I. Svoboda, H. Fuess, The crystal structure of Solid Perrhenic Acid Monohydrate, Z. Anorg. Allg. Chem. 619 (1993) 1679–1681. https://doi.org/10.1002/zaac.19936191007.

[4] H.A. Evans, Y. Wu, R. Seshadri, A.K. Cheetham, Perovskite-related ReO_3-type structures, Nat. Rev. Mater. 5 (2020) 196–213. https://doi.org/10.1038/s41578-019-0160-x.

[5] L.F. Mattheiss, Band Structure and Fermi Surface of ReO_3, Phys. Rev. 181 (1969) 987–1000. https://doi.org/10.1103/PhysRev.181.987.

[6] M.G. Stachiotti, F. Cor`a, C.R.A. Catlow, C.O. Rodriguez, First-principles investigation of ReO_3 and related oxides, Phys. Rev. B 55 (1997) 7508–7514. https://doi.org/10.1103/PhysRevB.55.7508.

[7] A. Ferretti, D.B. Rogers, J.B. Goodenough, The relation of the electrical conductivity in single crystals of rhenium trioxide to the conductivities of Sr_2MgReO_6 and Na_xWO_3, J. Phys. Chem. Solids. 26 (1965) 2007–2011. https://doi.org/10.1016/0022-3697(65)90237-4.

[8] T.P. Pearsall, C.A. Lee, Electronic transport in ReO_3: dc conductivity and Hall effect, Phys. Rev. B 10 (1974) 2190–2194. https://doi.org/10.1103/PhysRevB.10.2190.

B. Polyakov, E. Butanovs, A. Ogurcovs, S. Vlassov, M. Zubkins, I. Jonane, A. Cintins, A. Kalinko, A. Kuzmin, J. Purans, Understanding the conversion process of magnetron-deposited thin films of amorphous ReOx to crystalline ReO3 upon thermal annealing, Cryst. Growth Des. 20 (2020) 6147-6156. https://doi.org/10.1021/acs.cgd.0c00848

[9] C.N. King, H.C. Kirsch, T.H. Geballe, The low temperature heat capacity and electrical resistivity of ReO_3, Solid State Commun. 9 (1971) 907–910. https://doi.org/10.1016/0038-1098(71)90510-2.

[10] T. Tanaka, T. Akahane, E. Bannai, S. Kawai, N. Tsuda, Y. Ishizawa, Role of polar optical phonon scattering in electrical resistivities of LaB_6 and ReO_3 (metallic conduction), J. Phys. C: Solid State Phys. 9 (1976) 1235–1241. https://doi.org/10.1088/0022-3719/9/7/014.

[11] P.B. Allen, W.W. Schulz, Bloch-Boltzmann analysis of electrical transport in intermetallic compounds: ReO_3, $BaPbO_3$, $CoSi_2$, and Pd_2Si, Phys. Rev. B. 47 (1993) 14434–14439. https://doi.org/10.1103/PhysRevB.47.14434.

[12] A. Fujimori, N. Tsuda, Electronically induced lattice distortion in WO_3 and stability of ReO_3 lattice, Solid State Commun. 34 (1980) 433–435. https://doi.org/10.1016/0038-1098(80)90645-6.

[13] A. Kuzmin, J. Purans, G. Dalba, P. Fornasini, F. Rocca, A high-temperature x-ray absorption spectroscopy study of ReO_3, J. Phys.: Condens. Matter. 8 (1996) 9083–9102. https://doi.org/10.1088/0953-8984/8/46/013.

[14] J.-E. Jørgensen, J. Staun Olsen, L. Gerward, Phase transitions in ReO_3 studied by high-pressure X-ray diffraction, J. Appl. Crystallogr. 33 (2000) 279–284. https://doi.org/10.1107/S0021889899016659.

[15] K. Biswas, D.V.S. Muthu, A.K. Sood, M.B. Kruger, B. Chen, C.N.R. Rao, Pressure-induced phase transitions in nanocrystalline ReO_3, J. Phys. Condens. Matter. 19 (2007) 436214. https://doi.org/10.1088/0953-8984/19/43/436214.

[16] J. Purans, G. Dalba, P. Fornasini, A. Kuzmin, S. De Panfilis, F. Rocca, EXAFS and XRD Studies with Subpicometer Accuracy: The Case of ReO_3, in: AIP Conf. Proc., AIP, Stanford, California (USA), 2007: pp. 422–424. https://doi.org/10.1063/1.2644546.

[17] T. Chatterji, P.F. Henry, R. Mittal, S.L. Chaplot, Negative thermal expansion of ReO_3: Neutron diffraction experiments and dynamical lattice calculations, Phys. Rev. B. 78 (2008) 134105. https://doi.org/10.1103/PhysRevB.78.134105.

[18] M. Dapiaggi, A.N. Fitch, Negative (and very low) thermal expansion in ReO_3 from 5 to 300 K, J. Appl. Crystallogr. 42 (2009) 253–258. https://doi.org/10.1107/S002188980804332X.

[19] K. Biswas, C.N.R. Rao, Metallic ReO_3 Nanoparticles, J. Phys. Chem. B. 110 (2006) 842–845. https://doi.org/10.1021/jp055670b.

[20] Y.Y. Chong, W.Y. Fan, Facile Synthesis of Single Crystalline Rhenium (VI) Trioxide Nanocubes with High Catalytic Efficiency for Photodegradation of Methyl Orange, J. Colloid Interface Sci. 397 (2013) 18–23. https://doi.org/10.1016/j.jcis.2013.01.030.

[21] W. Zhang, G. Deng, B. Li, X. Zhao, T. Ji, G. Song, Z. Xiao, Q. Cao, J. Xiao, X. Huang, G. Guan, R. Zou, X. Lu, J. Hu, Degradable rhenium trioxide nanocubes with high localized surface plasmon resonance absorbance

B. Polyakov, E. Butanovs, A. Ogurcovs, S. Vlassov, M. Zubkins, I. Jonane, A. Cintins, A. Kalinko, A. Kuzmin, J. Purans, Understanding the conversion process of magnetron-deposited thin films of amorphous ReOx to crystalline ReO3 upon thermal annealing, Cryst. Growth Des. 20 (2020) 6147-6156. https://doi.org/10.1021/acs.cgd.0c00848

like gold for photothermal theranostics, Biomaterials. 159 (2018) 68–81. https://doi.org/10.1016/j.biomaterials.2017.12.021.

[22] J.V. Rojas, C.H. Castano, Synthesis of rhenium oxide nanoparticles (Re_xO_y) by gamma irradiation, Radiat. Phys. Chem. 99 (2014) 1–5. https://doi.org/10.1016/j.radphyschem.2014.01.022.

[23] W. Wu, J. Yao, S. Liu, L. Zhao, L. Xu, Y. Sun, Y. Lou, J. Zhao, J.-H. Choi, L. Jiang, H. Wang, G. Zou, Nanostructured hexagonal ReO_3 with oxygen vacancies for efficient electrocatalytic hydrogen generation, Nanotechnology 30 (2019) 355701. https://doi.org/10.1088/1361-6528/ab214c.

[24] C. Diaz, M.L. Valenzuela, O. Cifuentes-Vaca, M. Segovia, M.A. Laguna-Bercero, Incorporation of Nanostructured ReO_3 in Silica Matrix and Their Activity Toward Photodegradation of Blue Methylene, J. Inorg. Organomet. Polym. Mater. 30 (2020) 1726–1734. https://doi.org/10.1007/s10904-019-01284-z.

[25] D. Myung, Y. Lee, J. Lee, H.K. Yu, J.-L. Lee, J.M. Baik, W. Kim, M.H. Kim, Synthesis of metallic ReO_3 nanowires, Phys. Status Solidi RRL - Rapid Res. Lett. 4 (2010) 365–367. https://doi.org/10.1002/pssr.201004417.

[26] W. Zhang, C. Yang, Z. Lei, G. Guan, S. He, Z. Zhang, R. Zou, H. Shen, J. Hu, New Strategy for Specific Eradication of Implant-Related Infections Based on Special and Selective Degradability of Rhenium Trioxide Nanocubes, ACS Appl. Mater. Interfaces. 11 (2019) 25691–25701. https://doi.org/10.1021/acsami.9b07359.

[27] M. Ohkubo, K. Fukai, M. Kohji, N. Iwata, H. Yamamoto, Preparation of conductive ReO_3 thin films, Supercond. Sci. Technol. 15 (2002) 1778–1780. https://doi.org/10.1088/0953-2048/15/12/332.

[28] M.G. Krishna, A.K. Bhattacharya, Growth of rhenium oxide thin films, Solid State Commun. 116 (2000) 637–641. https://doi.org/10.1016/S0038-1098(00)00386-0

[29] N.R. Murphy, R.C. Gallagher, L. Sun, J.G. Jones, J.T. Grant, Optical and chemical properties of mixed-valent rhenium oxide films synthesized by reactive DC magnetron sputtering, Opt. Mater. 45 (2015) 191–196. https://doi.org/10.1016/j.optmat.2015.03.035.

[30] W.A. Caliebe, V. Murzin, A. Kalinko, M. Görlitz, High-flux XAFS-beamline P64 at PETRA III, AIP Conf. Proc. 2054 (2019) 060031. https://doi.org/10.1063/1.5084662.

[31] J. Timoshenko, A. Kuzmin, J. Purans, EXAFS study of hydrogen intercalation into ReO_3 using the evolutionary algorithm, J. Phys. Condens. Matter. 26 (2014) 055401. https://doi.org/10.1088/0953-8984/26/5/055401.

[32] A. Kuzmin, J. Purans, M. Benfatto, C.R. Natoli, X-ray-absorption study of rhenium L_3 and L_1 edges in ReO_3: Multiple-scattering approach, Phys. Rev. B. 47 (1993) 2480–2486. https://doi.org/10.1103/PhysRevB.47.2480.

[33] A. Kuzmin, J. Chaboy, EXAFS and XANES analysis of oxides at the nanoscale, IUCrJ. 1 (2014) 571–589. https://doi.org/10.1107/S2052252514021101.

B. Polyakov, E. Butanovs, A. Ogurcovs, S. Vlassov, M. Zubkins, I. Jonane, A. Cintins, A. Kalinko, A. Kuzmin, J. Purans, Understanding the conversion process of magnetron-deposited thin films of amorphous ReOx to crystalline ReO3 upon thermal annealing, Cryst. Growth Des. 20 (2020) 6147-6156. https://doi.org/10.1021/acs.cgd.0c00848

[34] C.J. Howard, T.M. Sabine, F. Dickson, Structural and thermal parameters for rutile and anatase, Acta Crystallogr. B 47 (1991) 462–468. https://doi.org/10.1107/S010876819100335X.

[35] J. Timoshenko, A. Kuzmin, Wavelet data analysis of EXAFS spectra, Comput. Phys. Commun. 180 (2009) 920–925. https://doi.org/10.1016/j.cpc.2008.12.020.

[36] A.L. Ankudinov, B. Ravel, J.J. Rehr, S.D. Conradson, Real-space multiple-scattering calculation and interpretation of x-ray-absorption near-edge structure, Phys. Rev. B. 58 (1998) 7565–7576. https://doi.org/10.1103/PhysRevB.58.7565.

[37] J.J. Rehr, R.C. Albers, Theoretical approaches to x-ray absorption fine structure, Rev. Mod. Phys. 72 (2000) 621–654. https://doi.org/10.1103/RevModPhys.72.621.

[38] L. Hedin, B.I. Lundqvist, Explicit local exchange-correlation potentials, J. Phys. C: Solid State Phys. 4 (1971) 2064–2083. https://doi.org/10.1088/0022-3719/4/14/022.

[39] M.T. Greiner, T.C.R. Rocha, B. Johnson, A. Klyushin, A. Knop-Gericke, R. Schlögl, The Oxidation of Rhenium and Identification of Rhenium Oxides During Catalytic Partial Oxidation of Ethylene: An In-Situ XPS Study, Z. Phys. Chem. 228 (2014) 521–541. https://doi.org/10.1515/zpch-2014-0002.

[40] J. Okal, XPS study of oxidation of rhenium metal on γ-Al_2O_3 support, J. Catal. 225 (2004) 498–509. https://doi.org/10.1016/j.jcat.2004.05.004.

[41] K. Utsumi, O. Matsunaga, T. Takahata, Low resistivity ITO film prepared using the ultra high density ITO target, Thin Solid Films 334 (1998) 30–34. https://doi.org/10.1016/S0040-6090(98)01111-0.

[42] S. Kasap, C. Koughia, H.E. Ruda, Electrical Conduction in Metals and Semiconductors, in: S. Kasap, P. Capper (Eds.), Springer Handb. Electron. Photonic Mater., Springer International Publishing, Cham, 2017: pp. 1–1. https://doi.org/10.1007/978-3-319-48933-9_2.

[43] J. Feinleib, W.J. Scouler, A. Ferretti, Optical Properties of the Metal ReO_3 from 0.1 to 22 eV, Phys. Rev. 165 (1968) 765–774. https://doi.org/10.1103/PhysRev.165.765.

[44] J. Purans, P. Fornasini, S.E. Ali, G. Dalba, A. Kuzmin, F. Rocca, X-ray absorption spectroscopy study of local dynamics and thermal expansion in ReO_3, Phys. Rev. B. 92 (2015) 014302. https://doi.org/10.1103/PhysRevB.92.014302.

[45] K.V. Lawler, B.C. Childs, D.S. Mast, K.R. Czerwinski, F. Poineau, P.M. Forster, Molecular and Electronic Structures of M_2O_7 (M = Mn, Tc, Re), Inorg. Chem. 56 (2017) 2448–2458. https://doi.org/10.1021/acs.inorgchem.6b02503.

[46] H. Zhang, B. Chen, J.F. Banfield, G.A. Waychunas, Atomic structure of nanometer-sized amorphous TiO_2, Phys. Rev. B. 78 (2008) 214106. https://doi.org/10.1103/PhysRevB.78.214106.

B. Polyakov, E. Butanovs, A. Ogurcovs, S. Vlassov, M. Zubkins, I. Jonane, A. Cintins, A. Kalinko, A. Kuzmin, J. Purans, Understanding the conversion process of magnetron-deposited thin films of amorphous ReOx to crystalline ReO3 upon thermal annealing, Cryst. Growth Des. 20 (2020) 6147-6156. https://doi.org/10.1021/acs.cgd.0c00848

[47] C.A. Triana, C.M. Araujo, R. Ahuja, G.A. Niklasson, T. Edvinsson, Electronic transitions induced by short-range structural order in amorphous TiO_2, Phys. Rev. B. 94 (2016) 165129. https://doi.org/10.1103/PhysRevB.94.165129.

[48] J. Timoshenko, A. Kuzmin, J. Purans, Disappearance of correlations in the atom motion upon hydrogen intercalation into ReO_3 lattice, J. Phys.: Conf. Ser. 712 (2016) 012003. https://doi.org/10.1088/1742-6596/712/1/012003.

B. Polyakov, E. Butanovs, A. Ogurcovs, S. Vlassov, M. Zubkins, I. Jonane, A. Cintins, A. Kalinko, A. Kuzmin, J. Purans, Understanding the conversion process of magnetron-deposited thin films of amorphous ReOx to crystalline ReO3 upon thermal annealing, Cryst. Growth Des. 20 (2020) 6147-6156. https://doi.org/10.1021/acs.cgd.0c00848

FOR TABLE OF CONTENTS ONLY

Manuscript Title

Understanding of conversion process of magnetron deposited thin films of amorphous ReO_x to crystalline ReO_3 upon thermal annealing

Author list

Boris Polyakov[1], Edgars Butanovs[1], Andrejs Ogurcovs[2], Sergei Vlassov[3], Martins Zubkins[1], Inga Jonane,[1] Arturs Cintins,[1] Aleksandr Kalinko,[1,4] Alexei Kuzmin[1], Juris Purans[1]

[1]Institute of Solid State Physics, University of Latvia, Kengaraga Street 8, LV-1063 Riga, Latvia
[2]G. Liberts' Innovative Microscopy Centre, Department of Technology, Institute of Life Sciences and Technology, Daugavpils University, Parades street 1a, LV-5401 Daugavpils, Latvia
[3] Institute of Physics, University of Tartu, W. Ostwaldi Str. 1, 50412, Tartu, Estonia
[4] Department of Chemistry and Center for Sustainable Systems Design, Paderborn University, 33098 Paderborn, Germany

TOC Figure

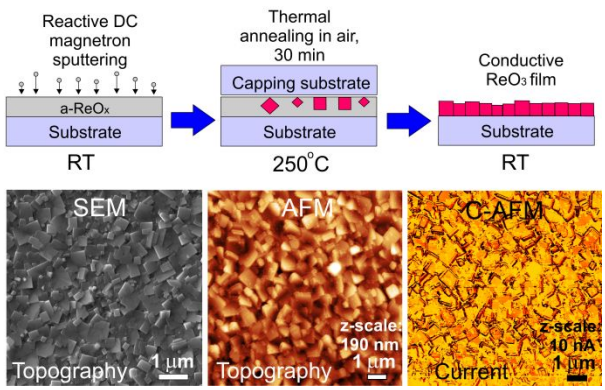

Synopsis

Thin films of rhenium trioxide (ReO_3) were produced by reactive DC magnetron sputtering from metallic rhenium target followed by annealing in the air in the range of temperatures from 200°C to 350°C. Optimal annealing temperature for ReO_3 thin films is 250°C.

Institute of Solid State Physics, University of Latvia as the Center of Excellence has received funding from the European Union's Horizon 2020 Framework Programme H2020-WIDESPREAD-01-2016-2017 TeamingPhase2 under grant agreement No. 739508, project CAMART²